

Aqueous secondary formation substantially contributes to hydrophilic organophosphate esters in aerosols

Received: 30 October 2024

Accepted: 15 April 2025

Published online: 14 May 2025



Shaojun Lv^{1,2,6}, LeLe Tian^{1,3,6}, Shizhen Zhao^{1,2}✉, Kevin C. Jones⁴,
Duohong Chen⁵, Guangcai Zhong^{1,2}, Jun Li^{1,2}, Buqing Xu¹,
Ping'an Peng^{1,2} & Gan Zhang^{1,2}✉

Chemicals of emerging concern (CECs), like organophosphate esters (OPEs), are toxic substances threatening human and wildlife health. Yet the atmospheric transformation of CECs remains poorly understood. Here we combine field measurements and partitioning models to reveal that OPEs could be enhanced by aqueous-phase processes in aerosols. We show that hydrophobic OPEs are absorbed favorably into the organic phase, whereas hydrophilic OPEs preferably partition into the aqueous phase. We provide field evidence that enhanced aqueous secondary formation of OPEs occurs in winter, and its magnitude is strongly dependent on aerosol water content. We suggest that dissolved inorganic salts and transition metals in aerosols positively impact the formation of particle-bound hydrophilic OPEs, by facilitating aqueous partitioning and/or oxidation. Our findings highlight the important role of aqueous oxidation chemistry for the fate of CECs in the atmosphere, urging better consideration of transformation products in future risk assessment and chemical management.

Chemicals of emerging concern (CECs) are known to pose serious threats to the health of organisms worldwide and are thus subject to the Stockholm Convention and the European REACH (Registration, Evaluation, Authorization and Restriction of Chemicals) framework^{1,2}. These hazardous chemicals have physicochemical properties that allow them to persist in the environment and undergo transformation processes, which leads to various transformation products (TPs), some even more toxic than their parent compounds². Apart from pesticides, a number of toxic TPs are not considered as part of chemical risk assessment in the European REACH regulation, despite their widespread presence worldwide³. However, the formation and transformation mechanisms of CECs in the complex real atmosphere remain poorly understood, hampering sufficient consideration given to the

atmospheric TPs generated from their parent CECs, in the existing framework of risk assessment and regulation.

Organophosphate esters (OPEs), as a group of CECs, are of increasing concern following the ban on polybrominated diphenyl ether flame retardants (PBDEs) by the Stockholm Convention in 2009. OPEs have become replacements for PBDEs, with the global consumption of OPEs increasing nearly a hundredfold from 2011 to 2019^{4,5}. OPEs in the atmosphere occur in gaseous and particulate adsorbed states, and the gas-to-particle partitioning determines the environmental fate of OPEs, including transport, deposition, and degradation⁶. Levels of OPEs in the air have been reported to be increasing in recent years, preferentially partitioning to the particle phase^{7,8}. Several empirical models based on vapor pressure (p_L^*) and the octanol-air

¹State Key Laboratory of Advanced Environmental Technology, Guangzhou Institute of Geochemistry, Chinese Academy of Sciences, Guangzhou, China.

²Guangdong-Hong Kong-Macao Joint Laboratory for Environmental Pollution and Control, Guangzhou Institute of Geochemistry, Chinese Academy of Sciences, Guangzhou, China. ³University of Chinese Academy of Sciences, Beijing, China. ⁴Lancaster Environmental Centre, Lancaster University, Lancaster, UK. ⁵Environmental Key Laboratory of Regional Air Quality Monitoring, Ministry of Ecology and Environment, Guangdong Environmental Monitoring Center, Guangzhou, China. ⁶These authors contributed equally: Shaojun Lv, LeLe Tian.

✉e-mail: zhaoshizhen@gig.ac.cn; zhanggan@gig.ac.cn

partition coefficient (K_{OA}) have been used to predict the partitioning of CECs, but differences in physicochemical properties complicate the interpretation of their results. For instance, most non-polar or less polar chemicals (e.g., PBDEs) are poorly water-soluble and can be reasonably estimated by all models⁹. However, the majority of highly polar OPEs have been observed to become very enriched on particles, contradicting predictions that suggest them to be mostly in the gas phase^{10,11}.

Particle-bound OPEs are generally believed to be dominated by the partitioning of primary OPEs, which originate from the volatilization, abrasion, and leaching of OPE-containing products during their production, use, and waste disposal¹². However, recent studies have detected OPEs as TPs formed by oxidation of organophosphate antioxidants (OPAs) in indoor dust and airborne particles, suggesting a possible secondary formation of OPEs^{13,14}. Meanwhile, laboratory and modeling studies have demonstrated a large contribution of OPA oxidation to OPE contamination^{15,16}. In the atmosphere, numerous oxidants and particulate components have complex influences on the uptake kinetics of organic gases and secondary organic aerosol (SOA) formation¹⁷. Yet, the occurrence and contribution of secondary formation of OPEs in the ambient atmosphere remain largely unknown. As with many other CECs, such gaps impede a complete understanding of the atmospheric fate of OPEs and hinder effective policy-making to reduce ecosystem and health risks.

In this study, intensive field observations in the Pearl River Delta (PRD) are combined with theoretical predictions (detailed in the Methods) to elucidate the partitioning behavior and formation pathway of OPEs. We report that the significant gap between the measured and estimated particle-phase fractions of OPEs partially results from their aqueous-phase processes in both summer and winter. Moreover, we reveal the potential impact of the ‘salting-in’ effect on the aqueous partitioning of OPEs in summer. We provide observational evidence for enhanced aqueous formation of highly polar OPEs (with higher solubility) in winter. Finally, we perform source apportionment of OPEs and analyze $\delta^{13}\text{C}$ isotopic fingerprinting of molecular tracers in four of China’s megacities, which further confirms the increasing importance of aqueous secondary formation for OPEs in the atmosphere.

Results and discussion

Dynamics of OPE chemical composition over the PRD in China

We analyzed 11 OPEs in both gas and particle phases at nine urban sites of the PRD during summer (June to July) and winter (January to February) in 2018 (Supplementary Fig. 1). The OPE compounds are classified as alkyl-OPEs (i.e., triethyl phosphate (TEP), tris(2-butoxyethyl) phosphate (TBEP), tris(2-ethylhexyl) phosphate (TEHP), tripropyl phosphate (TPPrP)), aryl-OPEs (i.e., triphenyl phosphate (TPHP), tricresyl phosphate (TCP), 2-ethylhexyl diphenyl phosphate (EHDPP)), and halo-OPEs (i.e., tris(1,3-dichloro-2-propyl) phosphate (TDCPP), tris(2-chloroethyl) phosphate (TCEP), tris(2-chloroisopropyl) phosphate (TCPP), tris(2,3-dibromopropyl) phosphate (TDBPP)). Detailed descriptions of the measurements are provided in the Methods.

The campaign-mean concentration of total atmospheric OPEs ($\Sigma_{11}\text{OPE}$ in the gas and particle phases) was $16 \pm 12 \text{ ng m}^{-3}$ in the PRD region, which was significantly higher than those reported in other regions (Supplementary Table 1)^{11,18,19}. The halo-OPEs comprised the major fraction of total OPEs in the atmosphere, followed by the aryl-OPEs and the alkyl-OPEs (Fig. 1a). TDBPP, which has been phased out of markets in many countries due to its high toxicity, accounted for only 11% of $\Sigma_{11}\text{OPE}$. Notably, three chlorinated OPEs (Cl-OPEs, i.e., TDCPP, TCEP, and TCPP) comprised, on average, 73% of $\Sigma_{11}\text{OPE}$ in the PRD region, which was comparable to other urban areas in China (Supplementary Fig. 2)^{11,18,19}. Such high Cl-OPE fractions in China are probably explained by their high usage and resistance to degradation²⁰.

We observed distinct seasonal differences in both OPE concentration and composition (Fig. 1a and Supplementary Table 2). First, the concentrations of gaseous and particulate OPEs in summer were much higher than those in winter, signifying that higher air temperature favors the release of OPEs from surface sources, such as the OPE-containing products, soils, water bodies and landfills²¹. Second, larger amounts of OPEs tend to accumulate in the particle phase than the gas phase, especially in winter. Third, in summer, the alkyl-OPEs, aryl-OPEs and halo-OPEs accounted for, on average, 1.1%, 15.4% and 83.6%, respectively, of the total OPE mass in the gas phase, and a similar pattern was observed in the particle phase (1.7%, 9.7% and 88.6%, respectively). However, in winter, while the mass fractions of alkyl-OPEs (16.2%) and aryl-OPEs (46.7%) in the gas phase were nearly twice as high as those in the particle phase (7.7% and 20.9%, respectively), the halo-OPE fraction in the gas phase (37.1%) was half that in the particle phase (71.4%).

We further investigated the relationship between particulate matter $\leq 2.5 \mu\text{m}$ ($\text{PM}_{2.5}$) and OPEs (Fig. 1b, c). The concentration of gaseous OPEs decreased with $\text{PM}_{2.5}$ loading ($R = -0.95$, $p < 0.05$), and the particle-bound OPEs were positively correlated with $\text{PM}_{2.5}$ ($R = 0.89$, $p < 0.05$) in summer, implying that the uptake of gaseous OPEs by aerosol is an important pathway for the formation of particle-bound OPEs. This is supported by the similar pattern of composition in the gas phase and particle phase, as mentioned earlier. However, no significant correlation was found between the gaseous OPEs and $\text{PM}_{2.5}$ in winter ($R = -0.04$, $p > 0.05$), even though the particle-bound OPEs remained correlated well with $\text{PM}_{2.5}$ ($R = 0.97$, $p < 0.05$). The nitrate (NO_3^-) fraction in winter accounted for nearly half of the water-soluble inorganic constituents, which was two times higher than that in summer (Supplementary Fig. 3). It can be inferred that SOA formation in winter would be driven by the increasing aerosol liquid water (ALW), since NO_3^- is more hygroscopic than sulfate (SO_4^{2-})²². This was further supported by the higher secondary organic carbon (SOC) mass fraction observed in winter (55%) than that in summer (42%). As shown in Supplementary Fig. 4, SO_4^{2-} was positively correlated with relative humidity (RH) in winter ($R = 0.63$, $p < 0.05$), whereas in summer, it displayed a negative correlation with RH ($R = -0.56$, $p < 0.05$) and positively correlation with atmospheric oxidants (O_x , the total concentration of ozone (O_3) and nitrogen dioxide (NO_2), i.e., $\text{O}_x = \text{O}_3 + \text{NO}_2$) ($R = 0.79$, $p < 0.05$). These different seasonal characteristics lead us to hypothesize that winter $\text{PM}_{2.5}$, containing a large fraction of hygroscopic ions, may have enhanced the formation of secondary species, which is consistent with previous studies^{23–25}. We, therefore, investigated in detail the role that gas-to-particle partitioning and formation processes play in the fate of OPEs in the atmosphere.

Gas-to-particle partitioning of OPEs

As shown in Supplementary Table 3, most highly polar OPEs ($p_L^\circ \geq 10^{-7} \text{ atm}$ and $\log K_{OA} < 8.5$), like TEP, TPPrP, TCEP, and TCPP, have high water solubility, ranging from 52 to $1.12 \times 10^4 \text{ mg L}^{-1}$, which are considered to be hydrophilic OPEs. Comparatively, the water solubility of less polar OPEs ($p_L^\circ < 10^{-7} \text{ atm}$ and $\log K_{OA} \geq 8.5$), like TBEP, TEHP, aryl-OPEs, and TDCPP, is 3 to 6 orders of magnitude lower than that of hydrophilic OPEs, and they can thus be regarded as hydrophobic OPEs. Herein, we applied the equilibrium absorptive partitioning theory to model the absorptive partitioning into the organic phase²⁶. The predicted particle-phase fraction of OPEs ($F_{p,t}$) was calculated from the corresponding gas-to-particle partitioning coefficient (K_{OM}) and the mass concentration of organic matter (OM) in aerosols (detailed in the Methods). The measured particle-phase fraction of OPEs ($F_{p,m}$) was calculated using the concentrations of OPEs in gas (C_g) and particle phase (C_p) (detailed in the Methods). $F_{p,t}$ with different p_L° datasets spans the gray-shaded region in Fig. 2a, b, of which the upper and lower limits are calculated using activity coefficients (ξ) corresponding to 0.3 and 3.0, respectively²⁷.

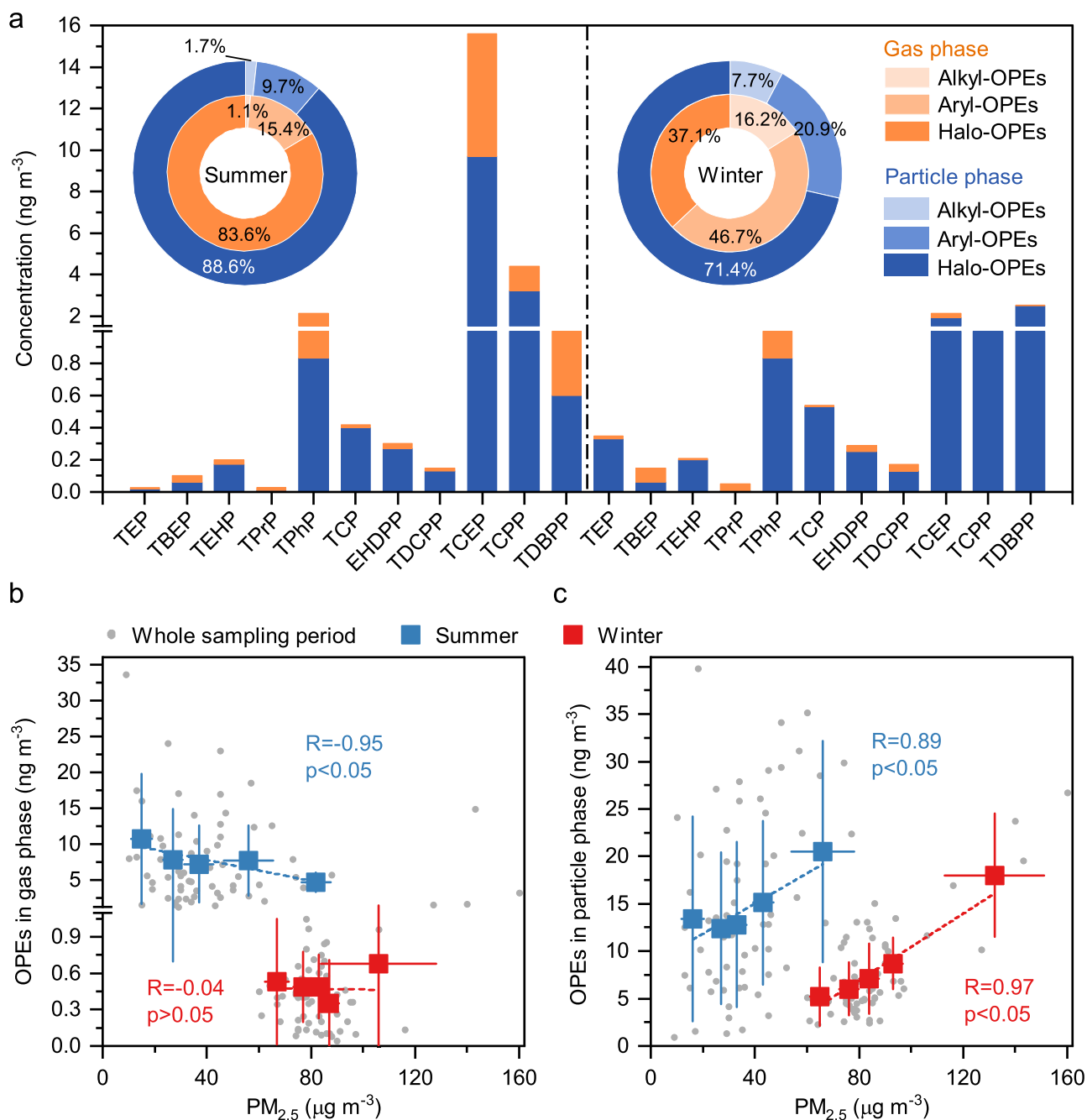


Fig. 1 | Composition profiles of OPEs and variation of OPEs as a function of PM_{2.5}. **a** Concentrations and relative contributions of alkyl-OPEs (i.e., TEP, TBEP, TEHP, and TPrP), aryl-OPEs (i.e., TPhP, TCP, and EHDPP), and halo-OPEs (i.e., TCEP, TCPP, TDCPP, and TDBPP) in gas phase and particle phase during summer and

winter. Relationships between the mass concentrations of PM_{2.5} and Σ_{11} OPEs in **(b)** gas phase and **(c)** particle phase in summer and winter. The square boxes and the error bars represent the mean values and standard deviation, respectively. The gray dots represent the concentration of total OPEs in the whole sampling period.

We found that the diversity of partitioning behaviors of OPEs was not determined by their functional groups, but was largely influenced by different physicochemical properties (Fig. 2a, b). The average $F_{p,m}$ of hydrophobic OPEs in both seasons was almost close to thermodynamic equilibrium partitioning, within the uncertainties of the measurements and calculations. This suggests that hydrophobic species have a greater tendency to associate with OM in PM_{2.5}. However, the mean $F_{p,m}$ of hydrophilic OPEs was much higher than their $F_{p,t}$, indicating that they did not preferentially partition into the organic phase of aerosols or gas phase, consistent with the previous results obtained from K_{OA} -based models^{7,10}. This phenomenon was previously explained, in part, by the influence of equilibrium sampling artifacts

such as gas-phase absorption onto filters⁹. However, the deviation caused by measurement uncertainties has been suggested to be much lower than the gap between theoretical and observed values²⁸, suggesting that OPEs may undergo other unknown mechanisms besides the sorption of OPEs onto a filter's water film.

The absorbing phase in PM_{2.5} is generally not a single organic phase, as it contains a substantial fraction of compounds that are highly hydrophilic and could form a concentrated solution in particles. Assuming that aerosols have a single phase, the total concentration of aerosols could be underestimated by 4 to 22% or even more²⁹. The aqueous-phase absorption of gaseous organics has been suggested to be an important formation pathway for SOA, which depends on their

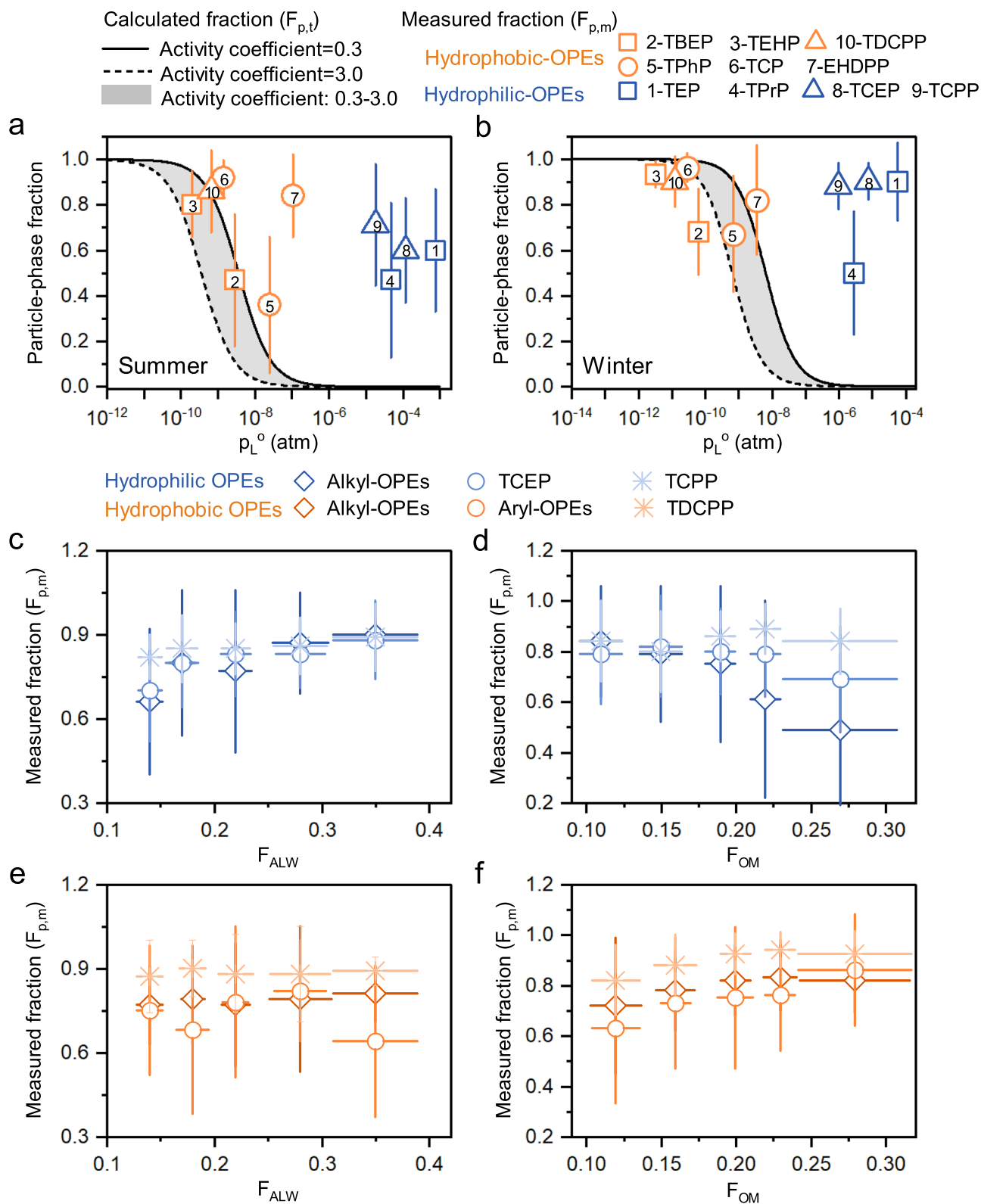


Fig. 2 | Modeling and observation of the gas-to-particle partitioning of hydrophilic and hydrophobic OPEs. a, b Comparison between the measured ($F_{p,m}$) and the calculated particle-phase fractions ($F_{p,t}$) of hydrophilic and hydrophobic OPEs by Pankow's absorptive theory during summer and winter; $F_{p,t}$ as a function of p_L^0 spans the gray-shaded region, where the upper and lower limits are

calculated using activity coefficients (γ) corresponding to 0.3 and 3.0, respectively. Measured particle-phase fractions of (c, d) hydrophilic (e, f) hydrophobic OPEs as a function of aerosol liquid water mass fraction (F_{ALW}) and organic matter mass fraction (F_{OM}) in $PM_{2.5}$. The error bars in (a–f) represent the standard deviation of the measured fraction values.

bulk solubility^{30,31}. To investigate the different phase partitioning of OPEs, we estimated the concentrations of ALW and OM in particles (“Methods”). A substantial increase in the $F_{p,m}$ of hydrophobic OPEs was associated with an elevated OM mass fraction in aerosols (F_{OM}) rather than the ALW loading (Fig. 2e, f). The mass fraction of nonpolar organics partitioning into the aqueous phase is negligible compared to that in the organic phase, despite the ALW being 2 to 3 times higher than the total aerosol dry mass^{32,33}. In contrast, the $F_{p,m}$ of hydrophilic OPEs positively responded to the increase in ALW mass fraction (F_{ALW}), but showed insignificant relationships with F_{OM} (Fig. 2c, d). This signifies that the partitioning of hydrophilic OPEs is very likely driven by the aqueous phase rather than the organic phase; this is consistent with an observation in the southeastern U.S., where the partitioning of water-soluble organics was highly dependent on ALW³⁴. It has also been suggested that gaseous water-soluble organics could have a stronger potential to partition in the aqueous phase compared to the organic phase³³.

To further investigate the aqueous absorption of OPEs, we calculated the field-derived effective Henry’s law coefficient ($K_{H,e}$, mol m⁻³ atm⁻¹) from measurement-based data (details in the Methods), which can be employed to describe the partitioning of gases to the aqueous phase. The $K_{H,e}$ of the OPEs in both seasons (10¹²–10¹⁴ mol m⁻³ atm⁻¹) was 5–12 orders of magnitude larger than the estimated Henry’s law coefficient in highly dilute solution ($K_{H,w}$, mol m⁻³ atm⁻¹) obtained from the Estimation Programs Interface Suite (Supplementary Table 4). The difference ($\Delta \log K_H$) between the measured $\log K_{H,e}$ and the recommended $\log K_{H,w}$ of hydrophobic OPEs has a strong dependence on $\log K_{OA}$ ($R = 0.81$, $p < 0.05$) and $\log K_{OW}$ ($R = 0.93$, $p < 0.05$) describing the partitioning capability of organics from gas phase to organic phase and from aqueous phase to organic phase, respectively (Supplementary Fig. 5). This further suggests that the organic phase may be more favorable for the absorption of hydrophobic OPEs. By contrast, the $\Delta \log K_H$ of hydrophilic OPEs was not significantly correlated with both $\log K_{OA}$ and $\log K_{OW}$ ($p > 0.05$), indicating little effect of organic-phase absorption on the partitioning of hydrophilic OPEs. The $\Delta \log K_H$ of hydrophilic OPEs was stable at approximately 6 and was comparable to or even greater than that of the carbonyl compounds (3–7) reported by Shen et al.³⁵. Since the aerosol containing water-soluble compounds is more hypersaline than pure water, the interactions among water, organic, and inorganic species in aerosol have been identified to be partially responsible for the enhanced partitioning to the condensed phase^{35,36}. Nevertheless, although there was no seasonal difference in the $\Delta \log K_H$ of hydrophilic OPEs, the $F_{p,m}$ values of most hydrophilic OPEs in winter were highly underestimated compared to those in summer (Fig. 2a, b).

Enhanced aqueous secondary formation of hydrophilic OPEs in winter

As discussed before, aqueous-phase processing might have imposed significant impacts on the formation of hydrophilic OPEs with a mean mass fraction of 72% in the total OPEs during the field campaign. Compared to TEP and TPrP, TCEP and TCPF have been demonstrated to be more stable OPEs in the atmosphere^{37,38}. Therefore, we selected TCEP and TCPF to further investigate the aqueous-phase formation pathways of hydrophilic OPEs. The concentrations of TCEP and TCPF in particle phase exhibited significant correlations with ALW ($R = 0.80$, $p < 0.05$) in winter (Supplementary Fig. 6a). They also tended to increase with the increase of 2-methylglyceric acid (2-MGA) serving as a tracer used to investigate the multiphase formation mechanisms of SOA³⁹. However, no significant correlation was observed in summer ($p > 0.05$) (Supplementary Fig. 6b), although the mass fractions of TCEP and TCPF in the hydrophilic OPEs exceeded 90% both in summer and winter. Therefore, the secondary formation of hydrophilic OPEs seems to take place preferentially in winter. A plausible mechanism for OPE formation in the atmosphere may be the oxidation of OPAs¹⁵. We

observed a significant correlation between O_x and particle-bound TCEP and TCPF ($R = 0.42$ – 0.79 , $p < 0.05$) in winter but no significant correlation in summer (Fig. 3a, b). This is consistent with previous laboratory studies on O_3 oxidation or photo-transformation of tris(2-chloroethyl) phosphite (TCEPi) on cover glass and dust^{15,40}. Although reports on the environmental occurrence and transformation behaviors of tris(2-chloropropyl) phosphite (TCPFi) are scarce, the correlation coefficient between TCPF and TCEP ($R^2 = 0.61$, $p < 0.05$) was higher than that of other OPEs (Supplementary Fig. 7), indicating that these two hydrophilic OPEs, with similar structures and physicochemical properties, may originate from similar sources or formation pathways. However, a higher concentration of ALW was observed in winter, particularly at the Guangzhou site, while the O_x concentration in winter was lower than that in summer (Supplementary Fig. 8), implying that the enhanced secondary OPE formation in winter may be influenced not only by oxidants but also by aqueous-phase processes in aerosols.

Aqueous-phase processes, including the absorption of precursors and aqueous oxidation, may play a key role in the secondary formation of hydrophilic OPEs in winter. Firstly, the concentration of succinic acid, which can be formed in the aqueous phase from lower molecular weight species via radical-radical reactions of carboxylic acids⁴¹, was higher in winter than that in summer (Supplementary Fig. 8). A highly positive correlation between the concentrations of hydrophilic OPEs and succinic acid in the particle phase was also evident in winter ($R = 0.82$, $p < 0.05$) (Fig. 3c). Secondly, the total concentrations of particle-bound TCEP and TCPF in winter tended to elevate with increasing SOC mass, whereas they showed much weaker relationships in summer (Fig. 3d). The SNA (comprising SO_4^{2-} , NO_3^- and ammonium (NH_4^+)) levels in winter were higher ($22 \pm 8.1 \mu g m^{-3}$) than those in summer ($8.5 \pm 5.7 \mu g m^{-3}$). At high SNA concentrations and increasing RH, aerosols may contain more water and become less viscous (Supplementary Fig. 9), favoring the accumulation of precursors and oxidants on the aerosol surface and ultimately facilitating the aqueous-phase reaction to form OPEs. Thirdly, the contribution of the condensation of gas-phase oxidation products could be excluded in winter, as the total mass of TCEP and TCPF in the gas phase did not show significant correlation with O_x ($R \leq 0.30$, $p > 0.05$), and their $PM_{2.5}$ -bound mass was not significantly correlated with $F_{p,m}$ ($R = 0.11$, $p > 0.05$) (Supplementary Fig. 10a, c). Moreover, their precursors (e.g., TCEPi and TCPFi) exhibit physicochemical properties (e.g., $\log K_{OA}$, $\log K_{OW}$, and water solubility) similar to those of OPEs (Supplementary Table 3 and Table 5), implying that hydrophilic precursors may be as dominated by aqueous partitioning as hydrophilic OPEs. The water solubility of their precursors is 3 to 6 orders of magnitude higher than that of hydrophobic OPAs, indicating that these hydrophilic precursors are more likely to partition into the aerosol aqueous phase, followed by aqueous oxidation. Recently, laboratory studies have suggested that the transformation of OPAs may be influenced by a number of key factors, including O_3 level, reactive oxygen species (ROS), and RH. For example, Liu et al. provided experimental evidence that OPA concentrations decreased significantly with increasing O_3 levels, accompanied by a high yield of the corresponding OPEs¹⁵. Similarly, Zhang et al. revealed that the heterogeneous transformation of OPAs in dust was accelerated in the presence of ROS and elevated RH⁴⁰. Consequently, the aqueous oxidation of precursors is likely the dominant process responsible for the secondary formation of hydrophilic OPEs in winter.

Transition metal elements (e.g., Fe and Mn) dissolved in the aqueous phase might play a crucial role in SOA formation, as they are expected to enhance the oxidative potential of O_3 by producing the ROS via Fenton chemistry⁴². The concentrations of Fe and Mn in winter were approximately twice as high as those in summer (Supplementary Fig. 8). The particle-bound TCEP and TCPF in winter were highly correlated with Fe and Mn ($R = 0.53$ – 0.79 , $p < 0.05$), especially at the

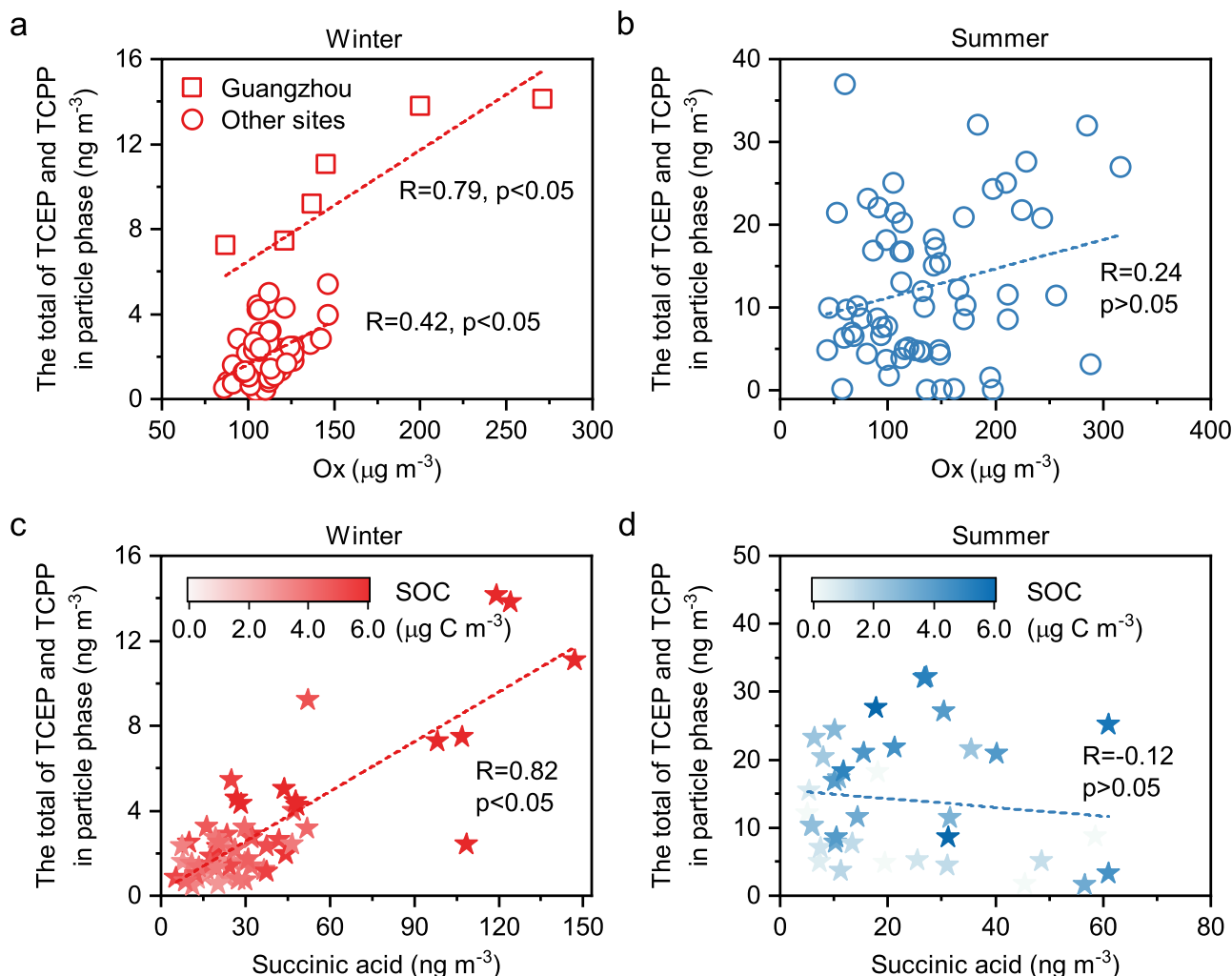


Fig. 3 | Relationships between hydrophilic OPEs in PM_{2.5} and secondary formation tracers. Correlations between the total concentration of TCEP and TCPP in particle phase and the concentrations of (a, b) O_x and (c, d) succinic acid in winter

and summer. The spots in (c, d) are colored according to the secondary organic carbon (SOC) concentrations.

Guangzhou site with higher ALW mass, while the weaker correlations were observed in summer ($R \leq 0.42$, $p < 0.05$) (Supplementary Fig. 6c–f), consistent with the aforementioned relationships between hydrophilic OPEs and O_x. The increased levels of transition metal elements and ALW possibly led to an enhanced conversion of gaseous oxidants to the condensed phase⁴³, thereby promoting the aqueous secondary formation of hydrophilic OPEs. This finding was in line with the conclusion of an experimental study that the oxidation of trimethyl phosphite with hydrogen peroxide (H₂O₂) in the presence of Fe salts occurred much faster than in the absence of an Fe-ions catalyst⁴⁴. Further laboratory investigations into the role of Fe-salts and Mn-salts aqueous chemistry in the secondary formation of OPEs, along with additional field measurements, are therefore suggested.

Gas-to-particle partitioning and salting-in effect in summer

In contrast to traditional persistent organic pollutants, aqueous-phase partitioning of gaseous hydrophilic OPEs may contribute more to the particle-bound OPEs in summer. The PM_{2.5}-bound TCEP and TCPP in summer were highly correlated with $F_{p,m}$ ($R = 0.62$, $p < 0.05$), while the gaseous mass was not significantly correlated with O_x ($p > 0.05$) (Supplementary Fig. 10b, d). This was consistent with the similar fraction characteristics of OPEs in gas and particle phases during summer (Fig. 1a), pointing to the partitioning of gaseous OPEs onto particles. The Henry's law-type partitioning of hydrophilic organics can

be enhanced by the 'salting-in' effect³⁶, which is defined as the negative slope (K_s) of the linear relationship between the salt concentration in aqueous phase and the logarithm of the ratio of $K_{H,w}$ and $K_{H,e}$ ($\log(K_{H,w}/K_{H,e})$). In Supplementary Fig. 11, the $\log(K_{H,w}/K_{H,e})$ values of TCEP and TCPP were regressed against the molality of SO₄²⁻ in ALW ($C_{SO_4^{2-}}$, mol kg⁻¹ ALW), since SO₄²⁻ has been recognized as a major factor for the salting effect of polar species^{28,35,36}. The K_s for TCEP and TCPP were observed to be significantly negative in summer ($p < 0.05$), with values of -0.06 and -0.09 , respectively, which fall within a similar range to that of carbonyl compounds and polyol tracers^{28,35}. The 'salting-in' effect was associated with the hydrophilic interactions, such as hydrogen bonding and water replacement, resulting in a decrease in Gibbs free energy or an increase in entropy^{36,45}. The enhanced partitioning of gaseous hydrophilic OPEs in summer might therefore be partially attributed to the 'salting-in' effect. However, the positive K_s values and weak correlations indicated that such an effect was not obvious in winter, likely due to competition from other formation pathways, such as aqueous oxidation.

Contribution of secondary formation to hydrophilic OPEs

To further confirm the importance of secondary formation to hydrophilic OPEs, we performed positive matrix factorization (PMF) to investigate the potential sources of hydrophilic OPEs in four megacities in China with active aqueous oxidation. Figure 4 showed the

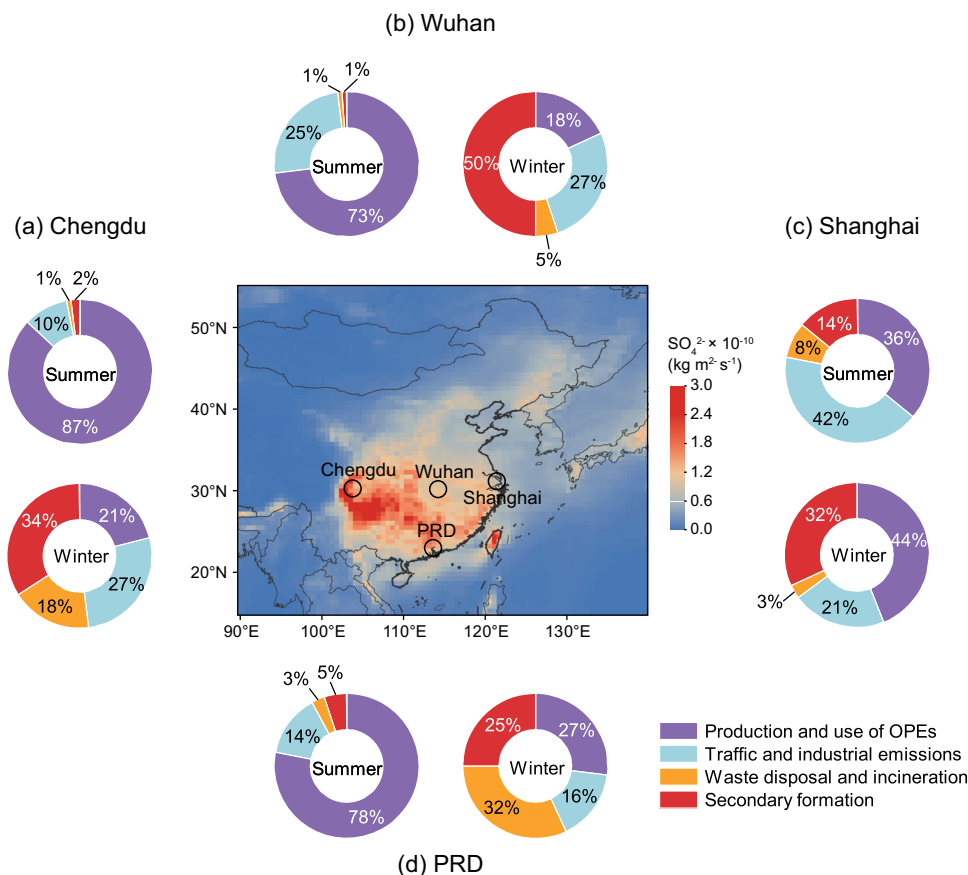


Fig. 4 | Sources of hydrophilic OPEs in $PM_{2.5}$. Relative contributions from production and use of OPEs, traffic and industrial emissions, waste disposal and incineration, and secondary formation sources to the mass concentrations of hydrophilic OPEs in (a) Chengdu, (b) Wuhan, (c) Shanghai and (d) the Pearl River Delta region (PRD) during summer and winter. Markers on the map show the measurement locations. The map is color-coded for the annual mean (January to

December 2018) of sulfate (SO_4^{2-}) production from aqueous sulfur dioxide (SO_2) oxidation. The data were obtained from Modern-Era Retrospective analysis for Research and Applications version 2 (MERRA-2) observations (<https://giovanni.gsfc.nasa.gov/giovanni/>). The base map of China and coastline boundaries in the map are originated from Meteoinfo free vector map data (<http://meteothink.org/downloads/index.html>).

locations of the sampling sites in a time-averaged map of SO_4^{2-} production from aqueous sulfur dioxide (SO_2) oxidation. A six-factor solution was achieved (Methods and Supplementary Fig. 12, 13). The first factor was characterized by a high abundance of TEHP (55%) and TPHP (83%), which was attributed to emissions from the electronic and lubricant products⁵. The second factor was dominated by TCEP (80%) and was identified as building construction emissions¹¹. The third factor showed a high abundance of TCPP (86%) and TDCPP (62%), and was identified as plastics and interior decoration emissions^{5,46}. Herein, the first, second, and third factors were collectively referred to as the production and use of OPEs. The fourth factor contained high loadings of metals (i.e., Sb, Pb, Cd, and As; 40–72%) that were associated with traffic and industrial sources⁴⁷. The fifth factor was dominated by the abundance of TDBPP (80%), phthalic acid (72%), and levoglucosan (82%). TDBPP, a widely used flame retardant additive for textiles, became obsolete in many countries and has been considered unused since 1970 due to its carcinogenicity and genotoxicity⁷. Previous studies suggested phthalic acid as an indicator of waste disposal emissions and levoglucosan as an indicator of combustion emission⁴⁸. Thus, the fifth factor was identified as waste disposal and incineration sources. Given that high fractions of secondary formation tracers (i.e., NO_3^- , SO_4^{2-} , NH_4^+ , and 2-MGA; 53–81%) were distinguished in the sixth factor, it was assigned as a secondary formation source^{39,49}.

As shown in Fig. 4, the emissions from production and use of OPEs were the dominant contributors to hydrophilic OPEs in summer (36–87%) across all urban sites, likely due to enhanced OPE release

from product surfaces under warmer conditions. The mixed source of traffic and industrial emissions contributed 10–42% and 16–27% to hydrophilic OPEs in summer and winter, respectively, highlighting their substantial impact on hydrophilic OPE levels. There were no significant seasonal differences in Wuhan and the PRD region, whereas Chengdu and Shanghai showed the opposite trend between summer and winter. Moreover, waste disposal and incineration emissions explained 3–32% of hydrophilic OPEs in winter, which was 3 to 10 times higher than that in summer (1–8%). The comparison among cities illustrates that the PRD and Chengdu are significantly affected by waste disposal and incineration emissions in winter.

More evidence supports the enhanced aqueous secondary formation of hydrophilic OPEs in winter. Firstly, the contribution of secondary formation showed a significant increase from summer (1–14%) to winter (25–50%). This indicated that an enhanced secondary formation of OPEs likely occurred in winter across China. Secondly, the sulfur oxidation ratio (SOR, $SOR = nSO_4^{2-} / (nSO_4^{2-} + nSO_2)$, where n represents the molar concentration), an indicator of atmospheric oxidation processes⁵⁰, was highly correlated with secondary hydrophilic OPEs to O_x ratio ((hydrophilic-OPEs)/ sec/O_x) in winter ($R = 0.62$, $p < 0.05$), while a weaker correlation was observed in summer ($R = 0.35$, $p < 0.05$) (Fig. 5a, b). Thirdly, we examined the relationship between $\delta^{13}C$ fingerprints of oxalic acid and (hydrophilic-OPEs)/ sec/O_x in Guangzhou, Chengdu, Wuhan, and Shanghai. The compound-specific $\delta^{13}C$ of oxalic acid is generally used as a tracer to differentiate various atmospheric chemical processes⁵¹. As illustrated in Fig. 5c, with

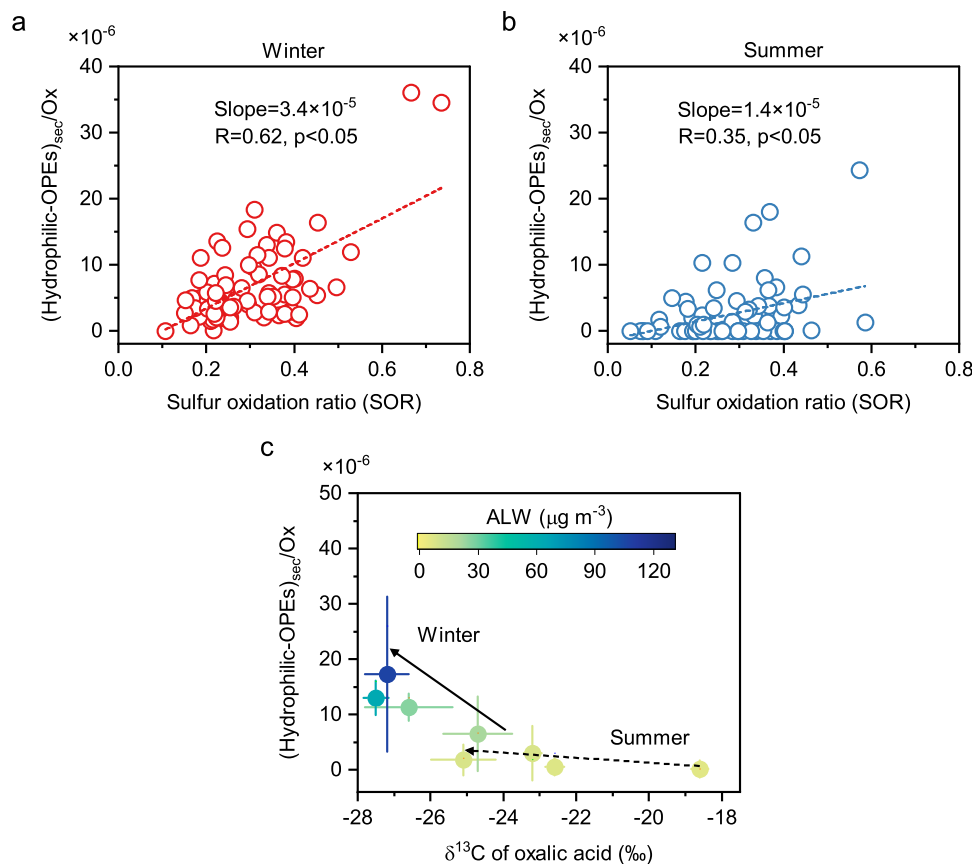


Fig. 5 | Variation of the secondary hydrophilic OPEs to O_x ratio ((hydrophilic-OPEs)_{sec}/ O_x) as a function of sulfur oxidation ratio (SOR) and $\delta^{13}C$ of oxalic acid. **a, b Correlations between (hydrophilic-OPEs)_{sec}/ O_x and SOR in winter and summer. **c** Relationships between (hydrophilic-OPEs)_{sec}/ O_x and $\delta^{13}C$ of oxalic**

acid in winter and summer for Guangzhou, Chengdu, Wuhan, and Shanghai. The spots in (c) are colored by aerosol liquid water (ALW) concentrations. The mass concentrations of secondary hydrophilic OPEs were obtained from the positive matrix factorization (PMF) model results.

increasing ALW, the higher generation of hydrophilic OPEs occurred with oxalic acid becoming more depleted in $\delta^{13}C$ in winter. On the contrary, (hydrophilic-OPEs)_{sec}/ O_x remained low regardless of the $\delta^{13}C$ reduction during summer. This was consistent with previous in situ observations of substantial water-soluble organic aerosols formed through secondary aqueous processes in megacities of China, especially in winter⁵¹. Taken together, these observations provide robust evidence for the growing importance of aqueous oxidation processes triggered by the elevated ALW in winter.

Atmospheric implications

The large contribution of aqueous-phase processes, including aqueous uptake and secondary formation of atmospheric OPEs, emphasized in this study, has important implications for accurate risk assessment and effective control of OPEs. Previous field and model studies focused on the partitioning behavior of OPEs between the gas and organic phase, but ignored the abundant aqueous phase in aerosols, resulting in the failure of K_{OA} -based models to accurately estimate the partitioning of hydrophilic OPEs (e.g., TCEP and TCPP)^{9,21}. Based on our observations, we reveal two distinct partitioning mechanisms of OPEs, characterized by the partitioning of hydrophobic species to the organic phase and the aqueous uptake of hydrophilic species, respectively. As for the sources of OPEs, current regulatory frameworks for OPEs generally pay more attention to the direct emission from OPEs used in commercial products, but does not consider the indirect contribution from OPAs^{15,16,52}. Our findings support the hypothesis that aqueous-phase oxidation of OPAs is a key pathway for hydrophilic OPE formation in the atmosphere.

As shown in Fig. 6, we illustrate two prominent effects of aqueous-phase processing on OPE formation in the atmosphere. First, particle-bound OPEs in summer are mainly driven by the gas-to-particle partitioning of gaseous contaminants emitted from primary sources. The high salt concentration (e.g., SO_4^{2-}) in the aqueous phase can promote the Henry's law-type partitioning process of OPEs via the 'salting-in' effect. Second, aqueous-phase reactions of OPAs and oxidants dominated TCEP and TCPP formation under polluted conditions during winter. Specifically, OPE precursors, such as TCEPi, first uptake into the aerosol aqueous phase through gas-to-particle partitioning, and subsequently undergo aqueous oxidation with O_3/O_2 to form TCEP. In the presence of abundant SNA in aerosols and increasing RH, enhanced ALW formation can facilitate the aqueous uptake of OPAs and oxidants, leading to greater OPE production in winter. In addition, the high fractions of Fe and Mn dissolved in the aqueous phase can enhance the oxidative potential of O_3 by generating ROS via Fenton chemistry, which may also be important for OPE formation. Therefore, these aqueous-phase processes can form an important, yet overlooked, driving force for OPE formation, especially with global warming and changes in atmospheric pollutants. Numerous studies have suggested that global warming can accelerate photochemical reactions to enhance O_3 formation^{53,54}. An increasing surface O_3 level has been observed in the PRD, YRD, and BTH regions, resulting in enhanced SOA formation^{55,56}. In addition, the ammonia-rich atmosphere in China, together with the slower decline rate of NO_x emissions and the effective sulfur emission control, has led to an increase in ALW and decreased aerosol viscosity, facilitating the aqueous-phase chemistry processes across China^{17,22}. Moreover, the rapid transition

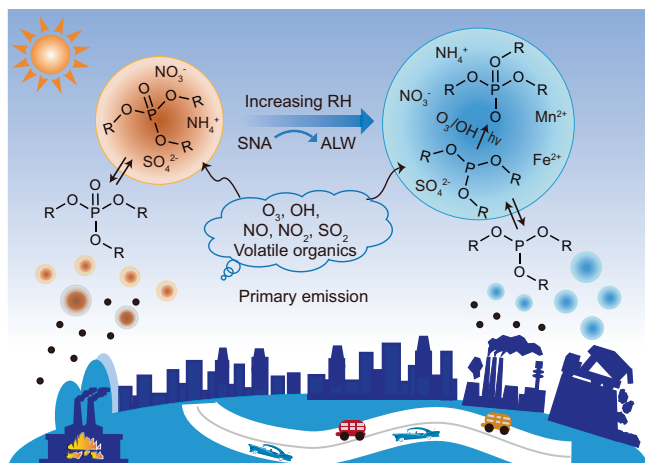


Fig. 6 | Conceptual diagram depicting the secondary formation of hydrophilic OPEs with increasing relative humidity (RH) and aerosol liquid water (ALW).

The left formation scheme illustrates the potential formation pathway of hydrophilic OPEs in summer, which is dominated by the partitioning of gas-phase OPEs emitted from primary sources. The right reaction scheme shows the secondary formation of hydrophilic OPEs via aqueous-phase oxidation of organophosphate antioxidants (OPAs), which is driven by high ALW triggered by increasing RH and SNA (comprising SO_4^{2-} , NO_3^- , and NH_4^+) concentrations in winter.

of energy structure from coal to natural gas in China was also expected to drive aerosols to be more hygroscopic, since natural gas combustion can generate three times more water vapor than coal burning⁵¹.

In addition to aerosol water, cloud/fog droplets are also important media for aqueous-phase reactions, where dissolved inorganic and organic gases are oxidized by various oxidants (e.g., singlet oxygen, O_3 , and hydroxyl radical)^{30,31}. These cloud/fog processes are generally accompanied by a liquid water content several orders of magnitude higher than ALW content, which has been demonstrated to enhance the formation of secondary species through accelerating aqueous-phase oxidation^{24,57}. Given that clouds cover nearly 70% of the Earth and the cloud/fog events frequently occur in winter^{58,59}, the role of cloud/fog chemistry in OPE formation should be undertaken for a better understanding of the atmospheric fate of OPEs. Note that the aqueous-phase processes in aerosol water or cloud/fog droplets are likely influenced by many factors. For example, transition metal elements (e.g., Fe, Mn) may catalyze OPE precursor oxidation via Fenton-like reactions in the aquatic environment⁶⁰. Recent evidence showed that O_3 -driven Fenton chemistry occurred four orders of magnitude faster on aqueous microdroplets than in bulk water⁴². A field study further suggested that Mn catalysis contributed up to 92.5% of SO_4^{2-} yields in North China's haze episodes⁶¹, highlighting the importance of metal-mediated pathways. While our results provide field evidence for the aerosol aqueous-phase formation of OPEs and its dependence on aerosol compositions, more laboratory-controlled studies are needed to better understand the factors influencing these aqueous-phase processes.

This study is limited by the scarcity of data on OPA production and use, as well as the technical challenges in measuring OPAs in aerosols, especially for TCPPI. Despite the high global production volume of total OPAs (up to 100,000 tons per year)¹⁵, data on the production and application of individual OPAs (e.g., TCPPI) remain unavailable. Moreover, the absence of reported environmental concentrations of TCPPI is a key limitation, which may reflect analytical challenges rather than its absence in the environment. TCEPI, including but not limited to it, has been detected in dust and soil but not in airborne fine particles, likely due to its rapid transformation in the atmosphere^{13,14,20}. To address these gaps, future studies urgently need to establish a comprehensive database of OPA production and

application and refine environmental monitoring methods for OPAs to further understand the secondary formation mechanism of OPEs in the atmosphere. While previous laboratory studies and our field observations provide insights into OPE formation mechanisms, upcoming research should prioritize integrating field measurements and laboratory simulations to better investigate aqueous-phase secondary formation pathways.

Our work provides important insights into the atmospheric fate of CECs and relevant air pollution control strategies, including but not limited to OPEs. First, CECs with different physicochemical properties show diverse gas-to-particle partitioning behaviors (e.g., organic- and aqueous-phase uptake), which should be considered in modeling studies to improve prediction accuracy. Second, failing to account for the aqueous secondary formation of CECs from parent chemicals could lead to an underestimation of the contribution of indirect sources and introduce uncertainties in risk assessment. Finally, a comprehensive and mechanistic understanding of CEC transformation processes would assist in improving TPs risk assessment and effectively addressing their hazards in chemical development and production, motivating refinements in future chemical management policies.

Methods

Sampling information

Sampling campaigns were conducted in nine cities in the PRD region (Supplementary Fig. 1): Guangzhou, Zhuhai, Shenzhen, Dongguan, Huizhou, Zhongshan, Jiangmen, Foshan, and Zhaoqing. The PRD region, as one of the representative megacity clusters, is the base of electronics and manufacturing industries in China, where high OPE concentrations have been observed⁶². In addition, active atmospheric chemical processing results in frequent O_3 pollution in the PRD region⁵⁵. Thus, these emission hotspots and strong atmospheric oxidation capacity provide a representative environment for the atmospheric transformation of OPEs. A total of 162 paired air samples were collected across 12 cities in China, comprising 126 samples from nine cities in the PRD region and 36 samples from three additional cities (Chengdu, Wuhan, and Shanghai). Each paired sample consisted of a quartz fiber filter (QFF, Whatman, 203 mm × 254 mm) for particle-phase collection and a polyurethane foam (PUF, 14 cm in diameter, 7.5 cm in thickness, and 0.02 g cm⁻³ in density) plug for gas-phase collection, using a high-volume active air sampler (Minya Instruments Co., Guangzhou, China). Sampling was conducted over 24-hour periods during summer (June–July 2018) and winter (January–February 2018), with 28 samples collected per city in the PRD region and 24 samples per city in the other three locations. To ensure data quality, four field blanks (24 PUF blanks and 24 QFF blanks) were collected at each sampling site to account for potential contamination during sampling.

Each QFF was baked at 450 °C for 8 h, and PUF was precleaned separately with acetone and dichloromethane before sampling. All samples were freeze-dried, packed, and stored at −20 °C. The concentrations of $\text{PM}_{2.5}$ were calculated by the gravimetric method. The meteorological parameters (RH and temperature) and the trace gas concentrations of O_3 , NO_x , and SO_2 were obtained from the corresponding official environmental monitoring stations at each sampling site, where trace gases were monitored using Thermo Scientific Environmental Instruments (models 49i, 42i, and 43i-TLE, respectively).

Chemical analysis and quality control

OPEs in gas- and particle-phase samples were determined using Soxhlet extraction combined with multi-segment column purification, and instrumental analysis⁷. QFFs and PUFs were spiked with TnBP-d₂₇ and TDCPP-d₁₅ as recovery surrogates and Soxhlet extracted for 24 h with dichloromethane (DCM). The extracts were reduced

and concentrated in a volume of 0.5–1 mL through nitrogen evaporation and solvent-exchanged into hexane. Multilayer silica gel was applied to purify the sample extracts and then eluted with 20 mL of DCM and acetone (1:1, v/v). The eluted solution was concentrated under nitrogen to a volume of 200 μL and spiked with TCEP-d₁₂ as an internal standard prior to instrumental analysis. Analysis of OPEs was performed using an gas chromatograph coupled to a mass selective detector (Shimadzu GCMS-QP2010), operated in negative chemical ionization under selected ion monitoring (SIM) mode with a DB-5MS column (30 m \times 0.25 mm \times 0.25 μm). The bulk components in PM_{2.5} including water soluble ions (i.e., SO_4^{2-} , NO_3^- , Cl^- , NH_4^+ , K^+ , Na^+ , Ca^{2+} and Mg^{2+}), organic tracers (e.g., levoglucosan, phthalic acid, succinic acid and 2-methylglyceric acid), metal elements (e.g., Fe, Sb, Cu, Pb and As), organic carbon (OC) and elemental carbon (EC), were measured for each filter sample. Detailed analytical methods of these compositions are given in the Supplementary Method 1.

For quality control, field blanks, procedural blanks, and surrogate-spiked recoveries were analyzed with each batch of samples to assess potential background contamination and instrumental performance. The reference ions for 11 OPEs and the corresponding labeled standards used in SIM mode on a Shimadzu GCMS-QP2010 and retention times (RT, min) are given in Supplementary Table 6. The instrumental detection limits (IDLs) and method detection limits (MDLs) of the target OPEs are provided in Supplementary Table 7. The average recovery rates of surrogates in samples were $86 \pm 21\%$ for TnBP-d₂₇, and $51 \pm 11\%$ for TDCPP-d₁₅. The detailed blank concentrations, including field and procedural blanks, were shown in Supplementary Table 8. The concentrations reported here were corrected for field blanks and recoveries.

Compound-specific $\delta^{13}\text{C}$ of oxalic acid

The PM_{2.5} filter was extracted with ultrapure water for three times and then concentrated to dryness. Subsequently, the extracts were derivatized with 10% boron trifluoride (BF_3) in 1-butanol in a water bath at 100 $^\circ\text{C}$ for about 1 hour, and then extracted with n-hexane. The $\delta^{13}\text{C}$ values of oxalic acid derivatives were analyzed using a gas chromatograph connected to an isotope ratio mass spectrometry (GC ISO-Link2/IRMS, Thermo Fisher Scientific). The $\delta^{13}\text{C}$ values of free oxalic acid were estimated by an isotopic mass balance method, based on the measured values and the $\delta^{13}\text{C}$ of the derivatizing agent (1-butanol, $\delta^{13}\text{C} = -30.21\text{‰}$). During derivatization, the isotopic fraction was found to be less than 0.73‰ in our previous studies⁶³. The difference in $\delta^{13}\text{C}$ of oxalic acid in replicate analyses was less than 1.0‰.

Calculations of partitioning coefficients

For each OPE compound, the theoretical partition coefficient (K_{OM}) for absorptive uptake into the organic phase can be calculated according to ref. 26:

$$K_{\text{OM}} = \frac{R \times T}{10^6 \times W_{\text{OM}} \times \xi \times p_{\text{L}}^0} \quad (1)$$

where R ($8.2 \times 10^{-5} \text{ m}^3 \text{ atm mol}^{-1} \text{ K}^{-1}$) is the ideal gas constant and T (K) is the ambient temperature. W_{OM} (set at 200 g mol^{-1} for all samples⁶⁴) denotes the average molecular weight of the absorbing phase. ξ is the activity coefficient of the compound in the absorbing phase. p_{L}^0 (atm) is the vapor pressure of the pure compound at the average ambient temperature. The particle-phase fraction of OPEs ($F_{\text{p,t}}$) based on Pankow's absorptive theory can be determined as ref. 26:

$$F_{\text{p,t}} = \left(1 + \frac{1}{K_{\text{OM}} \times C_{\text{OM}}} \right)^{-1} \quad (2)$$

where K_{OM} was calculated by the Eq. 1 and C_{OM} was the mass concentration of OM in aerosol ($C_{\text{OM}} = \text{OC} \times 1.8^{65}$). The measured particle-

phase fraction ($F_{\text{p,m}}$) was calculated by the mass concentrations of OPEs in gas and particle phases (C_{g} and C_{p} , ng m^{-3}) as follows:

$$F_{\text{p,m}} = \frac{C_{\text{p}}}{C_{\text{g}} + C_{\text{p}}} \quad (3)$$

The measurement-based effective Henry's law coefficient ($K_{\text{H,e}}$, $\text{mol m}^{-3} \text{ atm}^{-1}$) was calculated according to Qin et al.²⁸:

$$K_{\text{H,e}} = \frac{\rho_{\text{w}} \times C_{\text{p}}}{C_{\text{g}} \times R \times T \times [\text{ALW}]} \quad (4)$$

where C_{g} (ng m^{-3}) and C_{p} (ng m^{-3}) are gas- and particle-phase concentrations of OPEs, respectively. ρ_{w} (g cm^{-3}) is the density of water. R and T are the ideal gas constant and ambient temperature, respectively. ALW ($\mu\text{g m}^{-3}$) is the aerosol water content driven by inorganic (ALW_{i}) and organic components (ALW_{o}). The ALW_{i} was estimated using the ISORROPIA-II model, which was run in the metastable mode with meteorological parameters (T and RH) and the concentrations of inorganic ions (Na^+ , K^+ , NH_4^+ , Ca^{2+} , Mg^{2+} , Cl^- , NO_3^- , and SO_4^{2-})¹⁷. We excluded the data corresponding to $\text{RH} > 95\%$ and $\text{RH} < 40\%$, as extreme RH values can introduce high uncertainties in ALW_{i} prediction^{66,67}. The ALW_{o} was calculated using the following equation¹⁷:

$$\text{ALW}_{\text{o}} = \frac{C_{\text{OM}} \rho_{\text{w}} \cdot \kappa_{\text{org}}}{\rho_{\text{org}} \left(\frac{1}{\text{RH}} - 1 \right)} \quad (5)$$

where C_{OM} ($\mu\text{g m}^{-3}$) is the mass concentration of OM; ρ_{w} and ρ_{org} are the density of water ($\rho_{\text{w}} = 1.0 \text{ g cm}^{-3}$) and OM ($\rho_{\text{org}} = 1.4 \text{ g cm}^{-3}$), respectively; and κ_{org} is the hygroscopicity parameter for organic aerosol composition ($\kappa_{\text{org}} = 0.06$)⁶⁸.

The salting effects have been suggested to be an important factor for the Henry's law-type partitioning process of organic compounds^{28,35}. The salting effects can be described using the following equation³⁵:

$$\log \left(\frac{K_{\text{H,w}}}{K_{\text{H,e}}} \right) = K_{\text{s}} \times c_{\text{salt}} \quad (6)$$

where $K_{\text{H,w}}$ and $K_{\text{H,e}}$ are the Henry's law coefficients of the OPEs in pure water and in aerosol aqueous phase containing salts, respectively. K_{s} is the salting constant or Setschenow constant, where a negative value indicates a 'salting-in' effect, while a positive value means a 'salting-out' effect. C_{salt} is the concentration of salt in mol kg^{-1} ALW.

PMF model

Source apportionment of OPEs at the study sites was performed using a positive matrix factorization (PMF) model based on multivariate factor analysis. PMF has been widely used for source apportionment research of atmospheric pollutants. In this study, the mass concentrations of the measured organic species and inorganic ions, along with their associated uncertainty, were analyzed by PMF v5.0. The basic calculation formula of PMF is as follows:

$$X_{ij} = \sum_{m=1}^n G_{im} F_{jm} + E_{ij} \quad (7)$$

where X_{ij} represents the concentration of the j -th component of the i -th sample, n represents the number of factors, G_{im} represents the contribution rate of the m -th factor for the i -th sample, F_{jm} represents the fingerprint matrix of the main sources, that is, the content of the j -th component in the m -th factor, and E_{ij} is the residual matrix, representing the difference between the measured values and the model-estimated values.

Twenty-two species were input into PMF, including hydrophilic OPEs (the total of TCEP and TCPP), seven OPE species (i.e., TBEP, TEHP, TPHP, TCEP, TCPP, TDCPP and TDBPP), phthalic acid (PA) and levoglucosan (Levo.), eight metals (i.e., Zn, Sb, Pb, Cd, As, Cu, V and Mn), and four secondary formation tracers (2-MGA, NO₃⁻, SO₄²⁻ and NH₄⁺). Firstly, hydrophilic OPEs was set as a total variable and species weights were adjusted according to S/N, residual analysis, observed/predicted concentration correlation, and the Q values ($Q_{\text{true}}/Q_{\text{exp}}$) to determine the optimal source apportionment solution.

After iterative testing from two to eight factors in the preliminary runs, the six-factor solution was selected, as it yielded a $Q_{\text{true}}/Q_{\text{exp}}$ ratio of 5.4, corresponding to a relatively stable variation in $d(Q_{\text{true}}/Q_{\text{exp}})/dN$ (Supplementary Fig. 12a). The scaled residuals for almost all species ranged between -3 and 3, indicating that outliers did not influence the solution. As shown in Supplementary Fig. 12b, the observed and PMF-predicted concentrations of hydrophilic OPEs were in good agreement ($R^2 = 0.96$, $p < 0.05$). The factor profiles for the six-factor constrained run of the PMF analysis were shown in Supplementary Fig. 13. To evaluate the stability of the six-factor solution, bootstrapping (BS), displacement (DISP), and bootstrap combined with displacement (BS-DISP) were performed. As shown in Supplementary Table 9, 10, BS results of each factor were all above 90, and the DISP summary showed no observed drop of Q, and no error, and no swaps for $dQ_{\text{max}} = 4$ either. BS-DISP is a hybrid approach with a combination of the BS and DISP methods, showing 96% cases accepted. These uncertainty assessments confirm that the six-factor solution is both stable and reliable.

Data availability

The data underlying the findings of this study are deposited and are available in the Figshare digital repository (<https://doi.org/10.6084/m9.figshare.28541693>). The aerosol aqueous-phase sulfate production data from Modern-Era Retrospective analysis for Research and Applications version 2 (MERRA-2) used in this paper are openly available at <https://giovanni.gsfc.nasa.gov/giovanni/>. The base map of China and coastline boundaries in the map are originated from MeteorInfo free vector map data (<http://meteothink.org/downloads/index.html>). The administration boundaries in the map are originated from map products of the National Geomatics Center of China (<https://cloudcenter.tianditu.gov.cn/administrativeDivision>; Map review Number: GS(2024)0650).

References

- Rodgers, T. F. M., Giang, A., Diamond, M. L., Gillies, E. & Saini, A. Emissions and fate of organophosphate esters in outdoor urban environments. *Nat. Commun.* **14**, 1175 (2023).
- Liu, Q. et al. Uncovering global-scale risks from commercial chemicals in air. *Nature* **600**, 456–461 (2021).
- Zahn, D. et al. Should transformation products change the way we manage chemicals? *Environ. Sci. Technol.* **58**, 7710–7718 (2024).
- Wang, X., Zhu, Q., Yan, X., Wang, Y., Liao, C. & Jiang, G. A review of organophosphate flame retardants and plasticizers in the environment: Analysis, occurrence and risk assessment. *Sci. Total Environ.* **731**, 139071 (2020).
- Tian, Y. X., Chen, H. Y., Ma, J., Liu, Q. Y., Qu, Y. J. & Zhao, W. H. A critical review on sources and environmental behavior of organophosphorus flame retardants in the soil: Current knowledge and future perspectives. *J. Hazard Mater.* **452**, 131161 (2023).
- Yaman, B., Dumanoglu, Y. & Odabasi, M. Measurement and modeling the phase partitioning of organophosphate esters using their temperature-dependent octanol-air partition coefficients and vapor pressures. *Environ. Sci. Technol.* **54**, 8133–8143 (2020).
- Zhao, S. et al. Probing legacy and alternative flame retardants in the air of Chinese cities. *Environ. Sci. Technol.* **55**, 9450–9459 (2021).
- Zhang, W. et al. Spatial and temporal distribution of organophosphate esters in the atmosphere of the Beijing-Tianjin-Hebei region, China. *Environ. Pollut.* **244**, 182–189 (2019).
- Okeme, J. O., Rodgers, T. F. M., Jantunen, L. M. & Diamond, M. L. Examining the gas-particle partitioning of organophosphate esters: How reliable are air measurements? *Environ. Sci. Technol.* **52**, 13834–13844 (2018).
- Wu, Y., Venier, M. & Salamova, A. Spatiotemporal variations and partitioning behavior of organophosphate esters in the Great Lakes atmosphere. *Environ. Sci. Technol.* **54**, 5400–5408 (2020).
- Zhao, A. et al. Pollution profiles, influencing factors, and source apportionment of target and suspect organophosphate esters in ambient air: A case study in a typical city of Northern China. *J. Hazard Mater.* **444**, 130373 (2023).
- Wei, G.-L. et al. Organophosphorus flame retardants and plasticizers: Sources, occurrence, toxicity and human exposure. *Environ. Pollut.* **196**, 29–46 (2015).
- Liu, R. & Mabury, S. A. Organophosphite antioxidants in indoor dust represent an indirect source of organophosphate esters. *Environ. Sci. Technol.* **53**, 1805–1811 (2019).
- Liu, X. et al. Novel organophosphate esters in airborne particulate matters: Occurrences, precursors, and selected transformation products. *Environ. Sci. Technol.* **54**, 13771–13777 (2020).
- Liu, Q. et al. Oxidation of commercial antioxidants is driving increasing atmospheric abundance of organophosphate esters: Implication for global regulation. *One Earth* **6**, 1202–1212 (2023).
- Chen, R., Xing, C., Shen, G., Jones, K. C. & Zhu, Y. Indirect emissions from organophosphite antioxidants result in significant organophosphate ester contamination in China. *Environ. Sci. Technol.* **57**, 20304–20314 (2023).
- Lv, S. et al. Gas-to-aerosol phase partitioning of atmospheric water-soluble organic compounds at a rural site in China: An enhancing effect of NH₃ on SOA formation. *Environ. Sci. Technol.* **56**, 3915–3924 (2022).
- Rauert, C., Schuster, J. K., Eng, A. & Harner, T. Global atmospheric concentrations of brominated and chlorinated flame retardants and organophosphate esters. *Environ. Sci. Technol.* **52**, 2777–2789 (2018).
- Hao, Y. et al. Novel brominated and organophosphate flame retardants in the atmosphere of Fildes Peninsula, West Antarctica: Continuous observations from 2011 to 2020. *J. Hazard Mater.* **440**, 129776 (2022).
- Gong, X. et al. Organophosphite antioxidants in mulch films are important sources of organophosphate pollutants in farmlands. *Environ. Sci. Technol.* **55**, 7398–7406 (2021).
- Wang, Y., Bao, M., Tan, F., Qu, Z., Zhang, Y. & Chen, J. Distribution of organophosphate esters between the gas phase and PM_{2.5} in urban Dalian, China. *Environ. Pollut.* **259**, 113882 (2020).
- Lv, S. et al. Nitrate-enhanced gas-to-particle-phase partitioning of water-soluble organic compounds in Chinese Urban atmosphere: Implications for secondary organic aerosol formation. *Environ. Sci. Technol. Lett.* **10**, 14–20 (2023).
- Liu, T., Clegg, S. L. & Abbatt, J. P. D. Fast oxidation of sulfur dioxide by hydrogen peroxide in deliquesced aerosol particles. *Proc. Natl. Acad. Sci. USA* **117**, 1354–1359 (2020).
- Wang, J. et al. Fast sulfate formation from oxidation of SO₂ by NO₂ and HONO observed in Beijing haze. *Nat. Commun.* **11**, 2844 (2020).
- Wang, J. et al. Aqueous production of secondary organic aerosol from fossil-fuel emissions in winter Beijing haze. *Proc. Natl. Acad. Sci. USA* **118**, e2022179118 (2021).
- Pankow, J. F. An absorption-model of gas-particle partitioning of organic-compounds in the atmosphere. *Atmos. Environ.* **28**, 185–188 (1994).

27. Zhao, Y. et al. Insights into secondary organic aerosol formation mechanisms from measured gas/particle partitioning of specific organic tracer compounds. *Environ. Sci. Technol.* **47**, 3781–3787 (2013).
28. Qin, C. et al. Gas-particle partitioning of polyol tracers at a suburban site in Nanjing, east China: increased partitioning to the particle phase. *Atmos. Chem. Phys.* **21**, 12141–12153 (2021).
29. Erdakos, G. B. & Pankow, J. F. Gas/particle partitioning of neutral and ionizing compounds to single- and multi-phase aerosol particles. 2. Phase separation in liquid particulate matter containing both polar and low-polarity organic compounds. *Atmos. Environ.* **38**, 1005–1013 (2004).
30. McNeill, V. F. Aqueous organic chemistry in the atmosphere: Sources and chemical processing of organic aerosols. *Environ. Sci. Technol.* **49**, 1237–1244 (2015).
31. Ervens, B., Turpin, B. J. & Weber, R. J. Secondary organic aerosol formation in cloud droplets and aqueous particles (aqSOA): a review of laboratory, field and model studies. *Atmos. Chem. Phys.* **11**, 11069–11102 (2011).
32. Liao, H. & Seinfeld, J. H. Global impacts of gas-phase chemistry-aerosol interactions on direct radiative forcing by anthropogenic aerosols and ozone. *J. Geophys. Res. Atmos.* **110**, D18208 (2005).
33. Carlton, A. G. & Turpin, B. J. Particle partitioning potential of organic compounds is highest in the Eastern US and driven by anthropogenic water. *Atmos. Chem. Phys.* **13**, 10203–10214 (2013).
34. Hennigan, C. J., Bergin, M. H., Russell, A. G., Nenes, A. & Weber, R. J. Gas/particle partitioning of water-soluble organic aerosol in Atlanta. *Atmos. Chem. Phys.* **9**, 3613–3628 (2009).
35. Shen, H., Chen, Z., Li, H., Qian, X., Qin, X. & Shi, W. Gas-particle partitioning of carbonyl compounds in the ambient atmosphere. *Environ. Sci. Technol.* **52**, 10997–11006 (2018).
36. Waxman, E. M., Elm, J., Kurten, T., Mikkelsen, K. V., Ziemann, P. J. & Vokamer, R. Glyoxal and methylglyoxal setschenow salting constants in Sulfate, Nitrate, and Chloride solutions: Measurements and gibbs energies. *Environ. Sci. Technol.* **49**, 11500–11508 (2015).
37. Liu, Y., Liggio, J., Harner, T., Jantunen, L., Shoeib, M. & Li, S.-M. Heterogeneous OH initiated oxidation: A possible explanation for the persistence of organophosphate flame retardants in air. *Environ. Sci. Technol.* **48**, 1041–1048 (2014).
38. Wang, Y. et al. Organophosphate di- and tri-esters in indoor and outdoor dust from China and its implications for human exposure. *Sci. Total Environ.* **700**, 134502 (2020).
39. Lin, Y.-H. et al. Epoxide as a precursor to secondary organic aerosol formation from isoprene photooxidation in the presence of nitrogen oxides. *Proc. Natl. Acad. Sci. USA* **110**, 6718–6723 (2013).
40. Zhang, Q. et al. Organophosphite antioxidants and novel organophosphate esters in dust from China: Large-scale distribution and heterogeneous phototransformation. *Environ. Sci. Technol.* **57**, 4187–4198 (2023).
41. Tan, Y., Lim, Y. B., Altieri, K. E., Seitzinger, S. P. & Turpin, B. J. Mechanisms leading to oligomers and SOA through aqueous photooxidation: insights from OH radical oxidation of acetic acid and methylglyoxal. *Atmos. Chem. Phys.* **12**, 801–813 (2012).
42. Gu, A. Y., Musgrave, C., Goddard, W. A., Hoffmann, M. R. & Colussi, A. J. Role of ferryl ion intermediates in fast fenton chemistry on aqueous microdroplets. *Environ. Sci. Technol.* **55**, 14370–14377 (2021).
43. Qin, X. et al. Persistent uptake of H₂O₂ onto ambient PM_{2.5} via dark-fenton chemistry. *Environ. Sci. Technol.* **56**, 9978–9987 (2022).
44. Barton, D. H. R., Hill, D. R. & Hu, B. Catalysis of the oxidation of triphenylphosphine and of trimethyl phosphite by hydrogen peroxide in the presence of Fe-III compounds. *Tetrahedron Lett.* **38**, 1711–1712 (1997).
45. Sadeghi, R. & Jahani, F. Salting-In and Salting-Out of Water-Soluble Polymers in Aqueous Salt Solutions. *J. Phys. Chem. B* **116**, 5234–5241 (2012).
46. Yin, H., Liang, J., Wu, D., Li, S., Luo, Y. & Deng, X. Measurement report: Seasonality, distribution and sources of organophosphate esters in PM_{2.5} from an inland urban city in Southwest China. *Atmos. Chem. Phys.* **20**, 14933–14945 (2020).
47. Charron, A. et al. Identification and quantification of particulate tracers of exhaust and non-exhaust vehicle emissions. *Atmos. Chem. Phys.* **19**, 5187–5207 (2019).
48. Wang, X., Leung, C. W., Cai, Z. & Hu, D. PM_{2.5}-Bound Organophosphate Flame Retardants in Hong Kong: Occurrence, Origins, and Source-Specific Health Risks. *Environ. Sci. Technol.* **57**, 14289–14298 (2023).
49. Li, R. et al. Source apportionment of PM_{2.5} in Shanghai based on hourly organic molecular markers and other source tracers. *Atmos. Chem. Phys.* **20**, 12047–12061 (2020).
50. Han, Y. et al. Enhanced production of organosulfur species during a severe winter haze episode in the guanzhong basin of northwest China. *Environ. Sci. Technol.* **57**, 8708–8718 (2023).
51. Xu, B. et al. Large contribution of fossil-derived components to aqueous secondary organic aerosols in China. *Nat. Commun.* **13**, 5115 (2022).
52. Shi, J., Xu, C., Xiang, L., Chen, J. & Cai, Z. Tris(2,4-di-tert-butylphenyl)phosphate: An unexpected abundant toxic pollutant found in PM_{2.5}. *Environ. Sci. Technol.* **54**, 10570–10576 (2020).
53. Xie, F. et al. Improved global surface temperature simulation using stratospheric Ozone forcing with more accurate variability. *Sci. Rep.* **8**, 14474 (2018).
54. Wong, S., Wang, W. C., Isaksen, I. S. A., Bernsten, T. K. & Sundet, J. K. A global climate-chemistry model study of present-day tropospheric chemistry and radiative forcing from changes in tropospheric O₃ since the preindustrial period. *J. Geophys. Res. Atmos.* **109**, D11 (2004).
55. Wang, W. et al. Long-term trend of ozone pollution in China during 2014–2020: distinct seasonal and spatial characteristics and ozone sensitivity. *Atmos. Chem. Phys.* **22**, 8935–8949 (2022).
56. Liu, Y. et al. Increasing surface ozone and enhanced secondary organic carbon formation at a city junction site: An epitome of the Yangtze River Delta, China (2014–2017). *Environ. Pollut.* **265**, 114847 (2020).
57. Herrmann, H. et al. Tropospheric aqueous-phase chemistry: Kinetics, mechanisms, and its coupling to a changing gas phase. *Chem. Rev.* **115**, 4259–4334 (2015).
58. King, M. D., Platnick, S., Menzel, W. P., Ackerman, S. A. & Hubanks, P. A. Spatial and temporal distribution of clouds observed by MODIS Onboard the Terra and Aqua Satellites. *IEEE Trans. Geosci. Remote Sens.* **51**, 3826–3852 (2013).
59. Cai, S. Y. et al. Important role of low cloud and fog in Sulfate aerosol formation during winter haze over the North China Plain. *Geophys. Res. Lett.* **51**, e2023GL106597 (2024).
60. Qiu, H., Geng, J., Ren, H., Ding, L., Xu, K. & Zhang, Y. Aquatic transformation of phosphite under natural sunlight and simulated irradiation. *Water Res.* **109**, 69–76 (2017).
61. Wang, W. et al. Sulfate formation is dominated by manganese-catalyzed oxidation of SO₂ on aerosol surfaces during haze events. *Nat. Commun.* **12**, 1993 (2021).
62. Xie, Y. N. et al. Nitrate-dominated PM_{2.5} and elevation of particle pH observed in urban Beijing during the winter of 2017. *Atmos. Chem. Phys.* **20**, 5019–5033 (2020).
63. Xu, B. et al. Compound-specific radiocarbon analysis of low molecular weight dicarboxylic acids in ambient aerosols using preparative gas chromatography: Method development. *Environ. Sci. Technol. Lett.* **8**, 135–141 (2021).

64. Williams, B. J., Goldstein, A. H., Kreisberg, N. M. & Hering, S. V. In situ measurements of gas/particle-phase transitions for atmospheric semivolatile organic compounds. *Proc. Natl. Acad. Sci. USA* **107**, 6676–6681 (2010).
65. Malm, W. C. & Hand, J. L. An examination of the physical and optical properties of aerosols collected in the IMPROVE program. *Atmos. Environ.* **41**, 3407–3427 (2007).
66. Hennigan, C. J., Izumi, J., Sullivan, A. P., Weber, R. J. & Nenes, A. A critical evaluation of proxy methods used to estimate the acidity of atmospheric particles. *Atmos. Chem. Phys.* **15**, 2775–2790 (2015).
67. Guo, H. et al. Fine particle pH and the partitioning of nitric acid during winter in the northeastern United States. *J. Geophys. Res. Atmos.* **121**, 10355–10376 (2016).
68. Gunthe, S. S. et al. Cloud condensation nuclei (CCN) from fresh and aged air pollution in the megacity region of Beijing. *Atmos. Chem. Phys.* **11**, 11023–11039 (2011).

Acknowledgements

This work is supported by the National Natural Science Foundation of China (42107120 to S.Z. and 42030715 to G.Z.), the Alliance of International Science Organizations (ANSO-CR-KP-2021-05 to G.Z.), the Guangdong Basic and Applied Basic Research Foundation (2023B0303000007 to P.P., 2023B1515020067 to S.Z. and 2023A1515111185 to S.L.), the Youth Innovation Promotion Association of CAS (2022359 to S.Z.), and the Tuguangchi Award for Excellent Young Scholar GIG (TGC202204 to S.Z.). We sincerely thank the volunteers who contributed to the fieldwork.

Author contributions

S.Z. and G.Z. designed the research; S.L. analyzed the field data and led the writing; L.T. conducted the experiments; D.C. provided the field data, including meteorological parameters (RH and temperature) and trace gas concentrations (O_3 , NO_x and SO_2). K.C.J., G.C.Z., J.L., B.X. and P.P. contributed to manuscript review and editing.

Competing interests

The authors declare no competing interests.

Additional information

Supplementary information The online version contains supplementary material available at <https://doi.org/10.1038/s41467-025-59361-6>.

Correspondence and requests for materials should be addressed to Shizhen Zhao or Gan Zhang.

Peer review information *Nature Communications* thanks Xinlei Ge, and the other anonymous reviewer(s) for their contribution to the peer review of this work. A peer review file is available.

Reprints and permissions information is available at <http://www.nature.com/reprints>

Publisher's note Springer Nature remains neutral with regard to jurisdictional claims in published maps and institutional affiliations.

Open Access This article is licensed under a Creative Commons Attribution-NonCommercial-NoDerivatives 4.0 International License, which permits any non-commercial use, sharing, distribution and reproduction in any medium or format, as long as you give appropriate credit to the original author(s) and the source, provide a link to the Creative Commons licence, and indicate if you modified the licensed material. You do not have permission under this licence to share adapted material derived from this article or parts of it. The images or other third party material in this article are included in the article's Creative Commons licence, unless indicated otherwise in a credit line to the material. If material is not included in the article's Creative Commons licence and your intended use is not permitted by statutory regulation or exceeds the permitted use, you will need to obtain permission directly from the copyright holder. To view a copy of this licence, visit <http://creativecommons.org/licenses/by-nc-nd/4.0/>.

© The Author(s) 2025